
This is an electronic reprint of the original article.
This reprint may differ from the original in pagination and typographic detail.

Siren, Topias; Uotinen, Lauri; Rinne, Mikael; Shen, Baotang
Fracture Mechanics Modelling of an In Situ Concrete Spalling Experiment

Published in:
Rock Mechanics and Rock Engineering

DOI:
[10.1007/s00603-014-0646-1](https://doi.org/10.1007/s00603-014-0646-1)

Published: 01/01/2015

Document Version
Peer-reviewed accepted author manuscript, also known as Final accepted manuscript or Post-print

Published under the following license:
CC BY

Please cite the original version:
Siren, T., Uotinen, L., Rinne, M., & Shen, B. (2015). Fracture Mechanics Modelling of an In Situ Concrete Spalling Experiment. *Rock Mechanics and Rock Engineering*, 48(4), 1423-1438. <https://doi.org/10.1007/s00603-014-0646-1>

This material is protected by copyright and other intellectual property rights, and duplication or sale of all or part of any of the repository collections is not permitted, except that material may be duplicated by you for your research use or educational purposes in electronic or print form. You must obtain permission for any other use. Electronic or print copies may not be offered, whether for sale or otherwise to anyone who is not an authorised user.

Fracture mechanics modelling of an *in situ* concrete spalling experiment

Topias Siren*

Aalto University, Espoo, Finland

(topias.siren@aalto.fi)

Lauri Uotinen

Aalto University, Espoo, Finland

(lauri.uotinen@aalto.fi)

Mikael Rinne

Aalto University, Espoo, Finland

(mikael.rinne@aalto.fi)

Baotang Shen

CSIRO Earth Science and Resource Engineering, Brisbane, Australia

(baotang.shen@csiro.au)

*** Corresponding Author:**

Name: Topias Siren

Postal Address: Aalto University, PO Box 12100, 00076 Aalto, Finland

Tel: +358-50-3549 582

E-mail: topias.siren@aalto.fi

Abstract:

During operation of the nuclear waste disposal facility, some sprayed concrete reinforced underground spaces will be in use for approximately 100 years. During this time of use, the local stress regime will be altered by the radioactive decay heat. The change in the stress state will impose high demands on sprayed concrete, as it may suffer stress damage, or lose its adhesion to the rock surface. It is also unclear what kind of support pressure the sprayed concrete layer will apply to the rock. To investigate this, an *in situ* experiment is planned in the ONKALO underground rock characterization facility, at Olkiluoto, Finland. A vertical experimental hole will be concreted, and the surrounding rock mass will be instrumented with heat sources, in order to simulate increase in the surrounding stress field. The experiment is instrumented with an acoustic emission system for the observation of rock failure, temperature and strain gauges to observe the thermo-mechanical interactive behaviour of the concrete and rock at several levels, in both rock and concrete. A thermomechanical fracture mechanics study is necessary for the prediction of the damage before the experiment, in order to plan the experiment and instrumentation, and for generating a proper prediction/outcome-study due to the special nature of the *in situ* experiment. The prediction of acoustic emission pattern is created by Fracod 2D, and the model later compared to the actual observed acoustic emissions. The fracture mechanics model will be compared to a Comsol Multiphysics 3D model to study the geometrical effects along the hole axis.

Keywords: Sprayed concrete, Shotcrete, Compressive failure, Spalling, *In situ* experiment, Numerical modelling, Fracture mechanics, Rock Anisotropy, Thermal Spalling, Nuclear waste disposal

1 INTRODUCTION

During the operation of the Olkiluoto nuclear waste disposal facility, some sprayed concrete (shotcrete) reinforced underground spaces, such as shafts, will be in use for approximately 100 years, as the disposal operations will last approximately until 2120 (Saanio *et al.* 2012). The mechanical stability of sprayed concrete for a 100 year lifetime has not been fully studied, especially in conditions where the stress state is changed by nuclear waste disposal. The change in the stress state will impose high demands on the sprayed concrete reinforcement layer. It is possible that the sprayed concrete may suffer stress damage, or lose its adhesion to the rock surface. It is unclear what kind of support pressure the sprayed concrete will apply to the rock, and what will happen at the rock surface if the adhesion is lost.

The radioactive decay will continue throughout the whole operational time of the repository (Saanio *et al.* 2012). The decay heat production of the disposed canisters will be controlled to prevent thermal stress damage of the rock (Saanio *et al.* 2012). The deposition holes are filled with compressed blocks made from bentonite clay (buffer), and gaps between blocks and rock surface will be filled with bentonite pellets (Juvankoski 2013). The purpose of the bentonite buffer and pellets is to "support the deposition hole with its counter-pressure" (Juvankoski 2013). The deposition tunnels will be filled with backfill material, which is required to have sufficient swelling pressure to contribute to the stability of the tunnels (Keto *et al.* 2013). The maximum temperature of the bentonite buffer is limited to +100 °C (Ikonen & Raiko 2012).

The effect of support pressure in preventing rock spalling has been tested *in situ* by the Swedish Nuclear Fuel and Waste Management Company, and the tests have proved that the range of 10 to 20 kPa support pressure by LECA pellet filling of a 0.5 m diameter experimental hole will prevent spalling (Glamheden *et al.* 2010). Hakala *et al.* (2008) modelled the effect of buffer and backfill swelling pressure on the deposition hole and deposition tunnel, establishing that a

swelling pressure in the order of megapascals would be needed in order to prevent spalling. However, the support pressure caused by sprayed concrete, and the mechanical behaviour of sprayed concrete have not been studied in the nuclear waste disposal context.

The behaviour of sprayed concrete has been studied and modelled for example by Usman & Galler (2013), but usually with much larger sprayed concrete thicknesses. Usman & Galler modelled the long-term deterioration of a 200 mm thick sprayed concrete layer caused by "deterioration in the mechanical characteristics and aging of the rock" (Usman & Galler 2013). The rock type was marl, with very different mechanical behaviour compared to the hard crystalline rock of Olkiluoto. The pegmatitic granite and veined gneiss rocks at Olkiluoto in Finland are stiffer and more brittle, where typically sprayed concrete thicknesses between 40–100 mm are sufficient to withstand the excavation-induced and sub-critical deformations, plus supporting the loads caused by free wedges. Due to different sprayed concrete thicknesses and rock deformation behaviour, the methods usually applied for Alpine rocks are not usable in the hard crystalline rocks under consideration.

Although there is no published research data available for making conclusions, it can be reasonably assumed that, during the operation time, the local stress regime in the far-field region is significantly changed by the decay heat caused by the nuclear waste. The effects of a 4°C temperature increase at a depth of 415 m in a circular shaft was modelled and reported by Uotinen *et al.* (2013). The 4°C increase is assumed after 120 years operation in the central area of the technical rooms of the ONKALO underground facility, and it corresponds to approximately a 2 MPa increase of hydrostatic *in situ* stress. The maximum increase of tangential stresses in sprayed concrete is 3.65 MPa (Uotinen *et al.* 2013).

1.1 ICSE concrete spalling experiment

To investigate the behaviour of concrete in changed stress conditions, an *In situ* Concrete

Spalling Experiment (ICSE) is planned in the ONKALO underground rock characterization facility, Olkiluoto Finland (Fig. 1). A vertical experimental hole ONK-EH3 ($\varnothing=1.5$ m, $l=7.2$ m) will be concreted from hole level -3 m to its base, and the rock mass surrounding the experimental hole will be instrumented with eight vertical heat sources in order to simulate the increasing stress field due to decay heat. The experiment will simulate the shafts which may be reinforced using concrete. In the experiment concrete casting is used instead of sprayed concreting, which is unpractical to execute in the reasonably narrow experimental hole.

The upper part of the experimental hole consists mainly of pegmatitic granite, with a veined gneiss inclusion located at the lower part. In previous experiments, the gneiss inclusion has been observed to be more vulnerable in terms of visible damage, compared to the granitic component. In the planned experiment, the surroundings of the experimental hole are instrumented with an acoustic emission system to observe the rock failure during the experiment, with temperature and strain gauges to observe the thermo-mechanical behaviour between concrete and rock at several levels in both the rock and sprayed concrete.

A thermal fracture mechanics study is necessary for prediction of the damage before the experiment—in order to plan the experiment and instrumentation, and for the implementation of a proper prediction/outcome-study due to the special nature of this *in situ* experiment. Predictions developed for the pegmatitic and gneiss sections are presented in this article, together with comparative models without concrete, for studying the effect of the concrete support pressure. A prediction of acoustic emission pattern is made using the computer program Fracod 2D, and the results will be compared to the actual observed acoustic emissions. The results obtained from Fracod 2D fracture mechanics model are compared to the Comsol Multiphysics 3D model, based on the Finite Element Method (FEM), in order to study of the geometrical effects along the hole axis.

1.2 Experimental hole ONK-EH3

During the year 2013, the third phase of Posiva's Olkiluoto Spalling Experiment (POSE) was executed in the experimental hole ONK-EH3. In that experiment, a hole was heated from inside to induce spalling as stresses increase around the hole perimeter. The execution and outcome of the experiment are described in detail in a working report by Valli *et al.* (2014). Before the spalling experiment, several fractures initiated in the veined gneiss after one year caused by the boring of the experimental hole, implying time-dependent rock damage.

The damage caused in the spalling experiment to the experimental hole was visually minimal, with the main damage located in the veined gneisses. The pegmatitic granite remained visually intact, both before and during the spalling experiment. However, several acoustic emissions were observed from the pegmatitic granite, and there are indications of porosity increase (Valli *et al.* 2014). During the spalling experiment the fractures (Fig. 2) in the veined gneiss propagated further; however, no spalling was observed. After the experiment, the hole was scaled to establish the damage depth. The geology of the experimental hole with scaled damage areas in grey are sketched in Fig. 3 based on the 3D-photogrammetric model shown in Fig. 4.

2 THEORY

Fracod 5.0 is based on the Displacement Discontinuity (DD) method (Shen & Stephansson 1993). The basic theory behind the fracture mechanics code Fracod is further discussed in this Section.

2.1 Fracture propagation and initiation

A modified G-criterion, namely the F-criterion introduced by Shen & Stephansson (1993), is used as the fracture propagation criterion in Fracod. The F-criterion enables use of mixed mode

fracture propagation (Shen *et al.* 2014). The F-criterion for an arbitrary direction is formulated by the following formula (Shen *et al.* 2014):

$$F(\theta) = G_I(\theta)/G_{IC} + G_{II}(\theta)/G_{IIC} = 1.0 \quad (1)$$

where θ is the arbitrary direction, the G_I and G_{II} are the strain energy release rates in modes I and II respectively, and G_{IC} and G_{IIC} are the critical strain energy release rates. The use of an arbitrary direction in the equation enables the simulation of anisotropic rock masses. Critical values can be calculated as a function of the arbitrary direction, and fractures propagate in the most critical direction (Shen *et al.* 2014). In terms of fracture intensity and anisotropy, the F-criterion can be formulated as (Siren *et al.* 2011; Shen *et al.* 2014):

$$F(\theta) = (K_I/K_{IC}(\theta))^2 + (K_{II}/K_{IIC}(\theta))^2 = 1.0 \quad (1)$$

where K_I and K_{II} are the stress intensity factors in modes I and II respectively, and K_{IC} and K_{IIC} are the corresponding fracture toughness values.

The fracture initiation in Fracod is determined by the Mohr-Coulomb failure criterion, with a similar concept utilising direction dependent strength functions to adapt to the rock anisotropy (Shen *et al.* 2014).

The acoustic emission (AE) events are predicted using data from fracture propagation and fracture slip. The AE events can be predicted from location magnitude -6.0 M_L ; however, with the acoustic emission system installed around the experimental hole the lowest magnitude that can be recorded is -2.4 M_L (Reyes-Montes *et al.* 2014).

2.2 Thermo mechanical coupling

The constitutive thermo-elastic equations on which Fracod 2D is based, can be found for example from the works of Timoshenko & Goodier (1970). The thermo-elasticity is divided into constitutive equations for deviatoric and volumetric responses, of which the latter contains the thermal coupling terms. The thermal coupling is implemented using an indirect method,

which uses fictitious heat sources (Shen *et al.* 2014). The indirect method suits well the Displacement Discontinuity (DD) method used within Fracod 2D.

The coupling is implemented so that the thermal solution is calculated before the mechanical equations. The thermal stresses are calculated for each boundary element and added to boundary stresses. Finally the stresses and displacements are calculated for the internal points, with added thermal stresses and displacements.

2.3 Fracture toughness values for concrete

Reinhardt *et al.* (1997) conducted a number of laboratory tests for high strength concrete ($f_c = 85$ MPa), where they concluded that the K_{IC} is about one fifth of the K_{IIC} . This conclusion agrees well with numerical and experimental studies of Davies (1988), where he reported the K_{IIC} values to be between 1.8 to 2.0 MPa m^{-0.5}, and that K_{IIC} values were around seven times higher than the K_{IC} values ranging from 0.27 to 1.30 MPa m^{-0.5} reported by Swamy (1979). To combine these two observations, the following equation for the relation between K_{IC} and K_{IIC} in concrete can be derived:

$$K_{IC} = K_{IIC} / 6 \quad (1)$$

where K_{IC} and K_{IIC} are the mode I and II fracture toughness values respectively. Reinhardt *et al.* (1997) reported the relation between the average uniaxial compressive strength and the mode II fracture toughness K_{IIC} to be approximately as according to the following equation for concrete:

$$K_{IIC} = f_c / 19 \quad (2)$$

where f_c is the characteristic compressive strength of concrete in MPa and K_{IIC} is in MPa m^{-0.5}.

2.4 Dimensional reduction from the 3D to a 2D problem

Fracod 2D is a plane strain software, which can be described as an infinite medium solver. The actual problem has one open surface (floor of the tunnel above), and one quasi-infinite direction

(rock mass below) perpendicular to the horizontal calculation plane. Additionally, the tunnel above has an anisotropic geometry, and introduces an additional error due to the orthotropic response, which cannot be incorporated into the 2D model. In the 2D calculation geometry, there is an infinitely long circular hole, which is concreted along its full length. In the true geometry there is the tunnel above, which allows displacements and partial stress relaxation, and the sprayed concreting only covers from the -3 m level to the bottom of the hole. The tunnel above also has length, and along its length it can allow displacements, the floor rises, and modifies the surrounding rock mass thermal induced stress response from a symmetrical one to a more orthotropic condition.

The equivalent *in situ* stresses at 2D modelling levels were calculated using Examine 3D for both stress state interpretations. The problem is solved at the -3 m and -5 m levels, which are deep enough to mitigate the problem of the above open surfaces, but not deep enough to remove it completely. To study the error magnitude of the 3D effect, the problem was also modelled in 3D, by using Comsol Multiphysics 4.4 and the results were compared to those obtained from Fracod 2D.

3 MATERIALS AND METHODS

The geology of the investigation area consists of migmatitic gneisses with sub-horizontal pegmatitic veins. The foliation of the gneiss dips 52 degrees in the direction 175 degrees, with pegmatitic inclusions following the same trend. The first 4.5 metres of the experimental hole ONK-EH3 consists mainly of pegmatitic granite, with a minor veined gneiss intrusion at one metre depth on the eastern side of the hole (Fig. 4). At the bottom of the hole there is a significant veined gneiss intrusion, as can be seen in the panoramic geological map of the experimental hole in Fig 3. The gneiss intrusion is modelled with a discrete area, using the drillcore information at representative depths, with the notch that was scaled down after the

third phase of the POSE experiment.

Two depths are modelled: the pegmatitic granite at depth -3 m with and without concrete in order to investigate the support effects (Fig. 5 on the left), where the models are orientated perpendicular to the principal stress directions; and a model at approximately -5 m depth, with two lithological units (Fig. 5 on the right), where the models are orientated perpendicular to the cardinal directions. All models are run with two rock stress interpretations, creating in total six fracture mechanics models.

3.1 Rock stress

In the vicinity of the POSE niche, there are two different *in situ* stress state interpretations available, both based on LVDT-cell measurements. The earlier interpretation is from the access tunnel (VT1) at chainage 3620 m, and from the experimental niche before the excavation was enlarged to the full width of the final niche (at the time the niche was named EDZ niche). This interpretation is referred as EDZ & VT1 interpretation, and it resulted in 166° for the maximum principal stress direction. The latest prediction is based on LVDT-cell stress measurements conducted in the same experimental hole (ONK-EH3), where the concrete spalling experiment is planned to be executed. This interpretation is referred to as the ONK-EH3 interpretation, and it resulted in 120° for the maximum principal stress direction. The maximum principal stress around the experiment hole for the EDZ & VT1 interpretation is between 39 and 53 MPa (Fig. 6 on the left). For the ONK-EH3 stress interpretation, the maximum principal stress around the experiment hole is between 21 and 59 MPa (Fig. 6 on the right). These two stress interpretations are reported and explained in detail in Hakala & Valli (2013), and Valli *et al.* (2014).

In the 2D fracture mechanics prediction, the stress state below the tunnel floor must be calculated as an input parameter, because the 2D model in the horizontal plane cannot take into account the tunnel geometry above affecting the secondary stress field around the tunnel. The

two stress states were used in this study, the situation below the tunnel floor including the *in situ* and tunnel effect at a depth of -3 m, calculated by Siren (2011) for the EDZ & VT1 interpretation and Uotinen *et al.* (2013) for the ONK-EH3 interpretation. The stress state for -5 m depth is adopted from Hakala & Valli (2013). The secondary stress parameters are presented in Table 1; these are transformed to plane stresses expressed via σ_{xx} , σ_{yy} , τ_{xy} (see Table 2) to fit the perpendicular co-ordinate system of the models at -5 m depth. The *in situ* stresses are not assigned to the concrete layer.

The rock stress is increased using eight heaters placed in boreholes in the rock mass. The heating pattern in Fig. 7 is used in the modelling. In fracture mechanics, the heating is modelled in three-week steps, where the heating power from point sources in each time step is an average of the input values at the beginning and end of the time step. The boreholes where heating elements are installed are not modelled; the heat source is a point source within the rock mass. In the 2D model, a five percent heat flux from the concrete or rock surface in the middle of the model is applied for realism to model the heat loss via the hole upwards. For fractures, a zero heat flux is assumed as no water flow has been observed in the experimental hole. In the 3D model, no heat flux is applied, and the top surface is ideally insulated.

3.2 Rock properties

The parameters used for the rock mass (Table 3) were similar to those used in the thermomechanics prediction for the third phase of the POSE-experiment by Hakala & Valli (2013) in Table 3, complemented with data from various sources (Posiva 2012, Kukkonen *et al.* 2011, EN 1992-1-1:2004, SRMK C4: 2003, Neville 1995). The parameters required for the fracture mechanics prediction are presented in Table 4, obtained mostly from the work of Siren (2011 and 2012). In the upper parts of the experimental hole, the rock mass is assumed to be homogeneous, isotropic and linearly elastic pegmatitic granite, and the lower parts a

combination of pegmatitic granite and homogeneous, anisotropic and linearly elastic veined gneiss (Fig. 5). No laboratory testing was available for obtaining the fracture mechanics parameters of the sprayed concrete; therefore, literature references were used to determine the parameters described in the previous Section. The initial temperature of the rock is expected to be 18°C, after the third phase of the POSE experiment, in which the rock mass is expected to be heavily disturbed by the heating during the experiment.

The mean Poisson's ratio for pegmatitic granite is 0.29, and for gneiss 0.25, as reported by Posiva (2012). These ratios are used in the models at -5 m depth to generate differences between two lithological units. However, for the models at -3 m depth, Poisson's ratio 0.25 is used, as this is a mean value of the larger data set of 109 samples tested in veined gneiss and only 13 samples tested in pegmatitic granite. The elastic modulus for granites and gneisses is 60 GPa, but a lower 53 GPa value is used in modelling to fit the conditions for the rock already damaged by the third phase of the POSE heating experiment. 53 GPa was also used by Hakala & Valli (2013) in the 3D thermomechanical simulation of the third phase of the POSE experiment.

3.3 Concrete support pressure

The Swedish Nuclear Fuel and Waste Management Company has investigated the effect of support pressure to prevent rock spalling. Trials by SKB suggest that even a range of 10 to 20 kPa support pressure by LECA pellet filling of a 0.5 m diameter experiment hole will prevent spalling (Glamheden *et al.* 2010). The ability to generate support pressure via concrete will be studied in the ICSE experiment, and so the predictive fracture mechanics models are calculated without the concrete layer.

3.4 Concrete material properties

Concrete is a brittle material with a high compressive strength to tensile strength ratio. Concrete

surrounding the round hole will be completely under compression, and the relevant failure mode is compression-induced shear failure. The vicinity of the open surface causes the lowest principal stress to be zero, or small compared to the largest principal stress. By setting the confining stress to zero, and using the characteristic uniaxial compressive strength (f_{ck}) of concrete, we can easily obtain the tensile strength as half of the f_{ck} . For better numerical stability, the friction angle was set to a small value of 1° instead of zero. These assumptions are only valid for failure initiation of the thin concrete layers near open surfaces. For mechanical parameters (characteristic uniaxial compressive strength, tensile strength, elastic modulus and Poisson's ratio), the Eurocode 1992-1-1 values for C35-3/45-1 concrete strength grade were used.

For thermal properties, the density was based on quality assurance tests of reinforcement concrete used in the ONKALO facility. Thermal capacity, thermal conductivity and linear thermal expansion direct measurements were not available; therefore, literature values for concrete were used instead. As the mass of the sprayed concrete structure is small compared to the surrounding rock mass, the density, capacity and conductivity have little significance for the modelling results. However, the thermal expansion is the coupling factor between the thermal and mechanical models and directly influences the stresses. As the thermal expansion factors for concrete and PGR and VGN rocks are close to each other, the mechanical coupling effect is much more significant. The ratio of the elastic moduli is 1 : 1.56 for concrete to rock.

4 RESULTS

The models at -3 m depth are run using a special version of Fracod 5.0, slightly restricting tensile fracture displacements to enhance numerical stability during the final heating stages. The models at -5 m depth did not suffer problems with loose blocks; therefore the normal version of Fracod 5.0 could be used.

4.1 Temperature

The heating scheme is identical in all 2D models. The temperature distribution range is from 24 to 81°C after the first three weeks, 36 to 129°C after six weeks, and 20 to 179°C after 9 weeks (Fig. 8). The maximum temperature at heat sources is 179°C, however at a few centimetres from heat sources in the borehole wall, the temperature decreases to about 160°C. The temperature at the experimental hole wall is 58°C, 95°C and 134°C after 3, 6 and 9 weeks of heating respectively. The six weeks value roughly corresponds to the designed maximum temperature of 100 °C for the bentonite buffer, that is also the maximum temperature of the disposal hole. In the 3D model, temperatures (Fig. 9) match well with the fracture mechanics 2D prediction. The 3D model temperature patterns (Figs. 8 and 9) also agree well with the fracture mechanics 2D prediction.

4.2 Fracture initiation and propagation

The two stress interpretations produce similarly shaped fracture patterns, with respect to the principal stress directions. The principal stresses grow significantly between 6–9 weeks of heating (Fig. 10). The stresses in the fracture mechanics code become locally extremely high after the concrete failure, and these high stresses are not described in this paper because of the fracture tip interaction within the complex fracture geometry. Therefore, in Fig. 10, the stresses are plotted only between 100 and -10 MPa.

In the predictions from -3 m depth without concrete support, the fracturing initiates at the rock surface (upper rows in Figs. 11 and 12) in the first 3 weeks of heating, and expands later behind the rock surface—first in the direction of the minor principal stress, then all-around the experimental hole, finally forming a butterfly-shaped failure zone.

The concrete layer suffers a shear failure (lower rows in Figs. 11 and 12) in the first three weeks of heating. In the ONK-EH3 stress state, the failure progresses to rock surface already after

three weeks of heating, and the failure zone is large after nine weeks of heating with local 5 mm displacements; this is in contrast to the EDZ & VT1 stress interpretation, in which only minor fracture propagation was predicted to occur just after nine weeks of heating. The concrete fails slightly, only to the minor principal stress direction with the EDZ & VT1 stress interpretation, and the concrete structure remains coherent, whereas the failure covers all directions in the ONK-EH3 stress interpretation with lost structural integrity.

The models from -5 m depth (Fig. 5b), with one isotropic and one anisotropic rock are numerically challenging to compute, and computing times reached up to even weeks. The models became numerical unstable after three or six weeks of heating, due to the recursive nature of fracture mechanics, as the fractures started forming complicated spiral type patterns, which increased the maximum compressive and tensile stresses to unrealistic levels, at the maximum being over $1e+16$ MPa. Therefore, the results presented in Fig. 13 must be interpreted cautiously.

In the ONK-EH3 stress interpretation, the fracturing starts in all directions in pegmatitic granite, and in the veined gneiss in the direction of foliation from the sharp angle of the scaled notch. In the EDZ & VT1 stress interpretation, less fracturing is observed in veined gneiss. In both models, the failure concentrates in pegmatitic granite with only minor concrete failure.

4.3 Concrete support pressure

From the results (Figs. 11 and 12), it can be observed that the concrete clearly suppresses the rock damage. The predicted support pressure of concrete between weeks 3 and 6 using Fracod 2D, is from 1.3 MPa to a maximum of 2.4 MPa, in regions where the concrete is intact (Table 5). After 9 weeks of heating, the fracture mechanics prediction shows 3.0 MPa support pressure. The Comsol 3D model shows support pressures ranging from 2.6 MPa to 3.1 MPa at the -3 m level, after nine weeks of heating (Fig. 14).

4.4 Acoustic emissions

The predicted AE patterns for different calculation cases are presented in Fig. 15. Due to the large number of calculation cases, the ONK-EH3 case at -3 m depth is selected for AE result interpretation. In total, 15288 and 5569 local seismic magnitudes of $-2.4 M_L$ or larger acoustic emission events are predicted for unsupported and supported ONK-EH3 cases at -3 m depth respectively (Fig. 16). Lower than $-2.4 M_L$, events are probably too low to be recorded during the *in situ* experiment, based on the experience of Reyes-Montes *et al.* (2014) in the ONKALO. The spatial distribution and number of the acoustic emissions are comparable between the two stress scenarios, but according to Rinne *et al.* (2003) it is not reasonable to compare the predicted AE magnitudes with the measured magnitudes since the used element size is significantly larger than the rock grain size.

During three weeks of heating, the tangential stresses near the rock surface are for the unsupported case 58 MPa and for the supported case 31 MPa, compared to the tangential stress 68 MPa without fracture growth enabled (elastic model). During the following weeks of the experiment, the fracture growth causes anomalous stress distributions behind the rock surface, with locally high tangential (locally over 170 MPa) and tensile stresses. In locations where loose rock exists, the stresses are unrealistic and therefore discarded; however, loose rock enlarges the effective hole radius, increasing tangential stresses during the later stages of the experiment and increasing the tangential stresses compared to the elastic model. The concrete provides support pressure which can also be seen in the number of AE events, as the total number of AE events for the supported case is only 30 % of the unsupported case. The concrete failure after six weeks of heating almost triples the tangential stress (Fig. 16).

In the supported case, the events are slightly more evenly distributed between intervals, their percentages being 4 %, 16 %, 22 %, 24%, 34 % (Fig. 17a), compared to the unsupported case

7 %, 18 %, 18 %, 20 %, 36 % (Fig. 17b) which has slightly more higher magnitude events, and the number of accumulated AE events showing increased damage progression after nine weeks of heating. The number of AE events increases 28 % during the last three weeks of heating in the unsupported case.

4.5 Displacements

The displacement upward, towards the open surface, asymptotes at nine weeks to 1.9 mm in the 3D model. In the 2D model, this displacement cannot take place, and is converted into stresses instead. The 2D model is a conservative upper bound estimator for the *in situ* experiment. However, the shafts are long structures and the plane strain assumption is valid for them.

The maximum in-plane displacement in the 2D model is 7.4 mm in the concrete supported case with the ONK-EH3 stress state. The maximum displacement is located in the partial concrete failure. In the case of the EDZ & VT1 stress estimation, the concrete stays fairly intact and the maximum displacement reaches 1.6 mm. In the unsupported ONK-EH3 case, large loose 200 mm thick blocks, and, in the EDZ & VT1 case, several 20...50 mm thick blocks are formed after six weeks (Fig. 18).

5 CONCLUSIONS

The results from the Fracod 2D and Comsol 3D programs agree well, especially in the case of predicted temperatures, which will be higher in the experiment than expected during the operation of the spent nuclear fuel repository. Due to the high temperatures, the predictions suggest significant fracture growth, resulting in concrete and rock damage. Fracod 2D suggests that the concrete will fail before the rock, with the first failure occurring after three weeks of heating. The concrete layer provides significant support pressure up to 3 MPa, which is predicted to suppress the rock failure significantly. However, it is unclear what effect the loss of

adhesion at the concrete-rock interface will have. During the experiment, it will be monitored if the support pressure is enough to retain the damaged rock.

Models at -5 m depth suffer from the complexity created by three different materials in the models, and the complex geometry. The thin concrete layer would require the use of extremely small element sizes, which, combined with the complex geometry and material models, is computationally unobtainable. The concrete parameters will be tested during the execution of the ICSE experiment, which will give more confidence in terms of the modelling of thin concrete layers, as well as the results from the actual *in situ* experiment.

In the EDZ & VT1 model, the experimental hole is surrounded by a failure zone. The ONK-EH3 model without a concrete layer from the -3 m level, produces a distinctive butterfly-shaped failure zone, which has been discussed earlier, for example by Detournay & St. John (1988), and Martin *et al.* (1999). Shen & Barton (1997) modelled failure in a jointed rock mass with the 2D distinct element code UDEC, and this also resulted in large butterfly-shaped failure zones. Often these failures are not observed in tunnels, and are regarded as artefacts from numerical modelling. After Martin *et al.* (1999), butterfly-shaped failures require reasonably high stresses, as found at the Olkiluoto site. With the acoustic emission system installed around the experimental hole, it will be possible to monitor whether butterfly-shaped shear zones will propagate.

ACKNOWLEDGEMENTS

The authors wish to thank Matti Hakala, Jouni Valli and Charlotta Simelius for their excellent work reporting the third phase of the POSE experiment, which is the starting point for the ICSE experiment, and for the use of Figures 2, 4 and 6. The authors also wish to thank Ph.D. student Daniele Martinelli for his contribution to the ICSE experiment, Emer. Prof. John Hudson for advise and proofreading, M.Sc. Johannes Suikkanen for valuable conversations about fracture

mechanics and commenting on this paper, Posiva for their interest in and financial support of the research subject, the Confederation of Finnish Construction Industries RT and Aalto University for their support that financially enabled the writing of this article. The referenced Posiva's and SKB's reports can be downloaded from their websites, however the views expressed in this article are those of the authors and are not necessarily those of Posiva or SKB.

6 REFERENCES

- Davies J (1988) Numerical study of punch-through shear specimen in mode II testing for cementitious materials. *Int J Cem Compos & Lightw Concr* 10(1):3-14
- Detournay E, St John CM (1988) Design charts for a deep circular tunnel under non-uniform loading. *Rock Mech Rock Eng* 21(2):119- 137
- EN 1992-1-1:2004 (2004) Eurocode 2: Design of concrete structures. Part 1-1: General rules and rules for buildings. Finnish Standards Association SFS, Helsinki
- Glamheden R, Fälth B, Jacobsson L, Harrström J, Berglund, J, Bergkvist L (2010) Counterforce applied to prevent spalling. Swedish Nuclear Fuel and Waste Management Co, SKB Technical Report TR-10-37 (downloadable from <http://www.skb.se>), Stockholm
- Hakala M, Valli J (2013) ONKALO POSE experiment – Phase 3: 3DEC prediction. Posiva Oy, Working Report 2012-58 (downloadable from <http://www.posiva.fi>), Eurajoki
- Hakala M, Hudson J, Harrison J, Johansson E (2008) Assessment of the potential for rock spalling at the Olkiluoto site. Posiva Oy, Working Report 2008-83 (downloadable from <http://www.posiva.fi>), Eurajoki
- Ikonen K, Raiko H (2012). Thermal dimensioning of Olkiluoto repository for spent fuel. Posiva

- Oy, Working Report 2012-56 (downloadable from <http://www.posiva.fi>), Eurajoki
- Juvankoski M (2013) Buffer Design 2012. Posiva Oy, POSIVA Report 2012-14 (downloadable from <http://www.posiva.fi>), Eurajoki
- Keto P, Hassan M, Karttunen P, Kiviranta L, Kumpulainen S, Korkiala-Tanttu L, Koskinen V, Jalonen T, Koho P, Sievänen U (2013) Backfill Production Line 2012. Design, production and initial state of the deposition tunnel backfill and plug. Posiva Oy, POSIVA Report 2012-18 (downloadable from <http://www.posiva.fi>), Eurajoki
- Kukkonen I, Kivekäs L, Vuoriainen S, Kääriä M (2011) Thermal properties of rocks in Olkiluoto: Results of laboratory measurements 1994-2010. Posiva Oy, Working Report 2011-17 (downloadable from <http://www.posiva.fi>), Eurajoki
- SRMK C4:2003 (2003) The National Building Code of Finland: C4 Thermal insulation. Ministry of the Environment, (downloadable from <http://www.ymp.fi>), Helsinki
- Neville AM (1995) Properties of Concrete. Longman Group Ltd, London
- Martin CD, Kaiser PK, McCreath DR (1999) Hoek–Brown parameters for predicting the depth of brittle failure around tunnels. Canadian Geotechnical J. 36(1):136-151.
- Posiva (2012) Olkiluoto Site Description 2011. Posiva Oy, POSIVA Report 2011-02 (downloadable from <http://www.posiva.fi>), Eurajoki
- Reinhardt, H.W., Ošbolt ,J., Shilang, X., Dinku ,A. (1997) Shear of structural concrete members and pure mode II testing. Advanced Cement Based Materials 5(3):75-85.
- Reyes-Montes J, Flynn W, Huang J. (2014) ONKALO POSE Experiment – Phase 3: Acoustic and Ultrasonic Monitoring. Posiva Oy, Working report 2013-39 (downloadable from <http://www.posiva.fi>), Eurajoki

- Rinne M, Shen B, Lee H-S (2003) Äspö Hard Rock Laboratory. Äspö Pillar Stability Experiment. Modelling of fracture stability by Fracod. Preliminary results. Swedish Nuclear Fuel and Waste Management Co, International Progress Report IPR-03-05 (downloadable from <http://www.skb.se>), Stockholm
- Saario T, Ikonen A, Keto P, Kirkkomäki T, Kukkola T, Nieminen J, Raiko H (2012) Design of the Disposal Facility 2012. Posiva Oy, Working Report 2013-17 (downloadable from <http://www.posiva.fi>), Eurajoki
- Shen B, Barton N (1997) The disturbed zone around tunnels in jointed rock masses. *Int J Rock Mech Min Sci* 34:117-125
- Shen B, Stephansson O, Rinne M (2014) Modelling rock fracturing processes: a fracture mechanics approach using FRACOD. Springer, Berlin, 173 p, ISBN 978-94-007-6903
- Shen B, Stephansson O (1993) Numerical analysis of Mode I and Mode II propagation of rock fractures. *Int J Rock Mech Min Sci Geomech Abstr* 30(7):861-867
- Siren T, Shen M, Rinne K, Kemppainen K (2011) Numerical anisotropic fracture mechanics modelling in crystalline rock. In: Qian & Zhou (eds) *Harmonising Rock Engineering and the Environment*, Taylor & Francis Group, London, pp 535-539
- Siren T (2011) Fracture Mechanics Prediction for Posiva's Olkiluoto Spalling Experiment (POSE). Posiva Oy, Working report 2011-23 (downloadable from <http://www.posiva.fi>), Eurajoki
- Siren T (2012) Fracture Toughness Properties of Rocks in Olkiluoto: Laboratory Measurements 2008-2009. Posiva Oy, Working report 2012-25 (downloadable from <http://www.posiva.fi>), Eurajoki

Swamy R N (1979) Fracture mechanics applied to concrete. In: Lydon FD (ed) Developments in concrete technology, Part I, Applied Science Publishers Ltd, London, pp 221-281

Timoshenko SP, Goodier JN (1970) Theory of Elasticity. McGraw-Hill, New York

Uotinen L, Siren T, Martinelli D, Hakala M (2013) *In situ* experiment concerning thermally induced spalling of circular shotcreted shafts in deep crystalline rock. In: Proceedings of World Tunnel Congress 2013, Geneva, Switzerland

Usmann M, Galler R (2013) Long-term deterioration of lining in tunnels. International Journal of Rock Mech Min Sci. 2013;64: 84–89

Valli J, Hakala M, Wanne T, Siren T, Kantia P (2014) ONKALO POSE experiment – Phase 3: Execution and monitoring. Working Report 2013-41 (downloadable from <http://www.posiva.fi>), Eurajoki

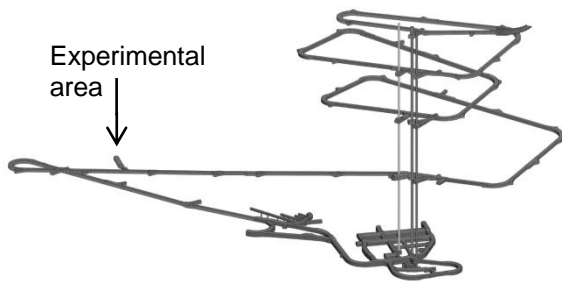


Fig. 1. Experimental area in the ONKALO underground facility.

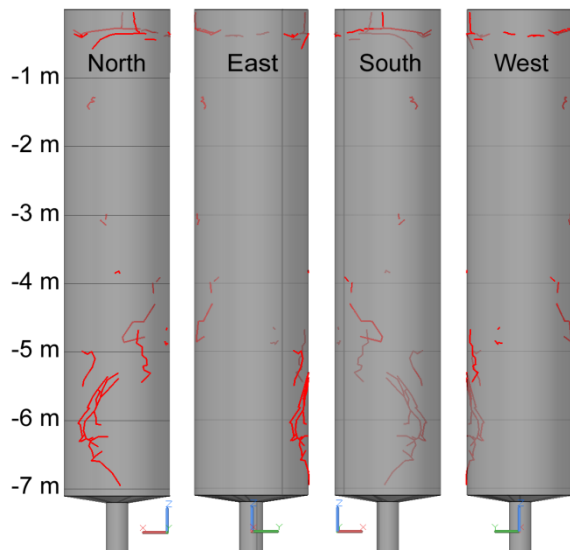


Fig. 2. The pre-existing fractures in 3D on the ONK-EH3 wall, viewpoints outside the hole. View from the north on the left, progressing through the cardinal directions to the right. (Valli *et al.* 2014)

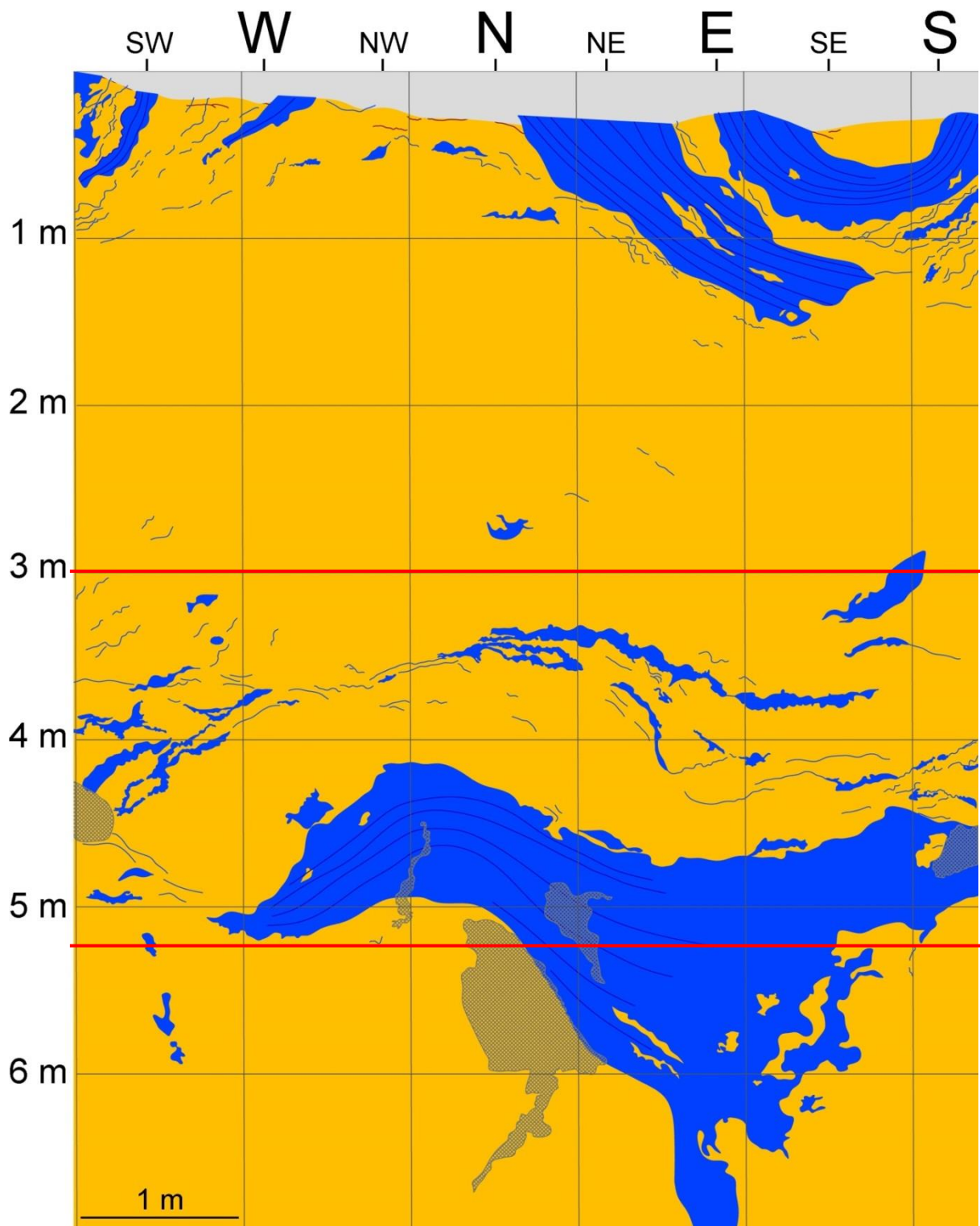


Fig. 3. A panoramic illustration of the experimental hole presenting the lithology with pegmatitic granite in orange, veined gneiss in blue, damage in grey and modelled planes in red. (Valli *et al.* 2014)

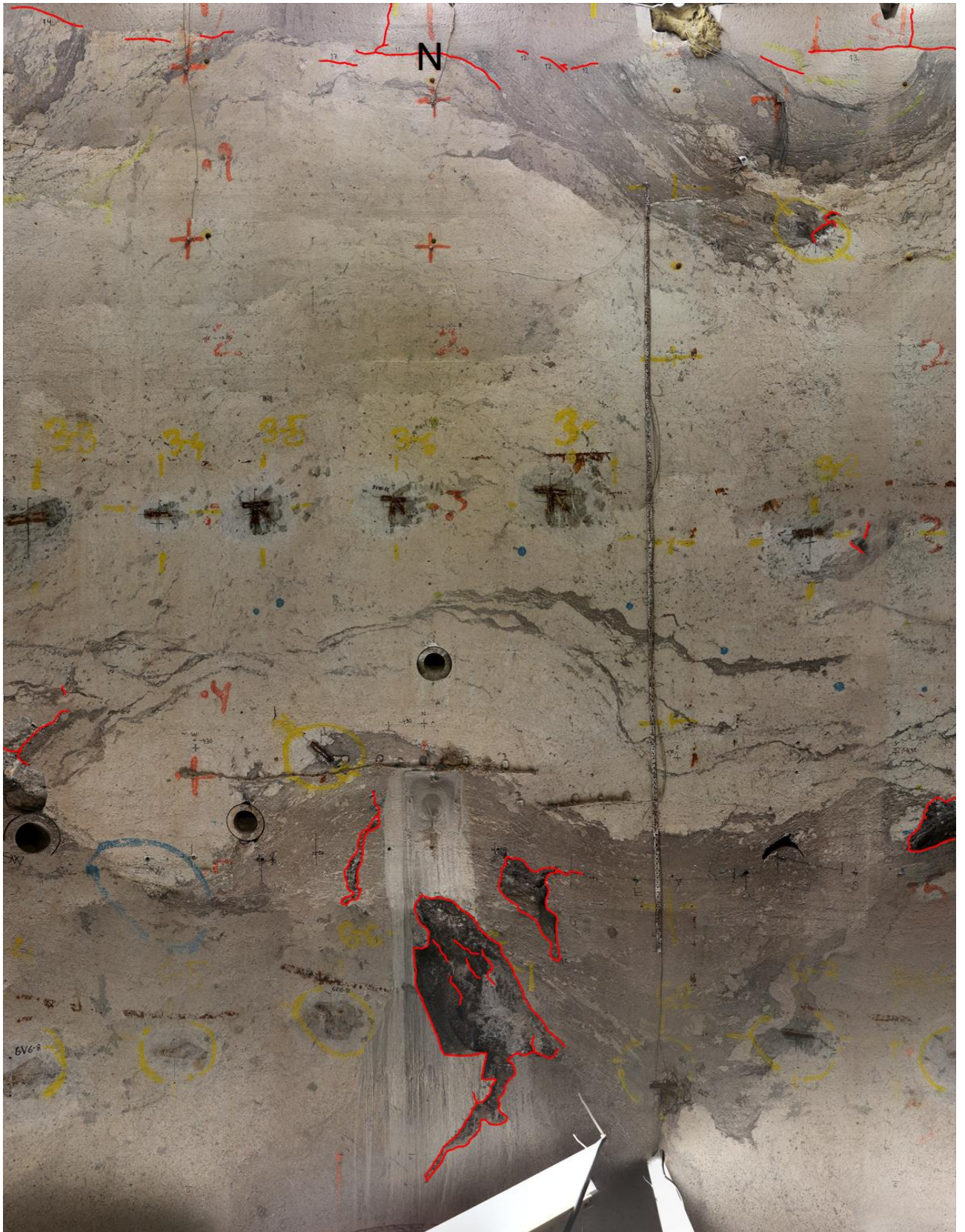


Fig. 4. Panoramic photograph of the experimental hole with fractures digitised in red. The white lines at the bottom of the hole are lights used in photographing. (Valli *et al.* 2014)

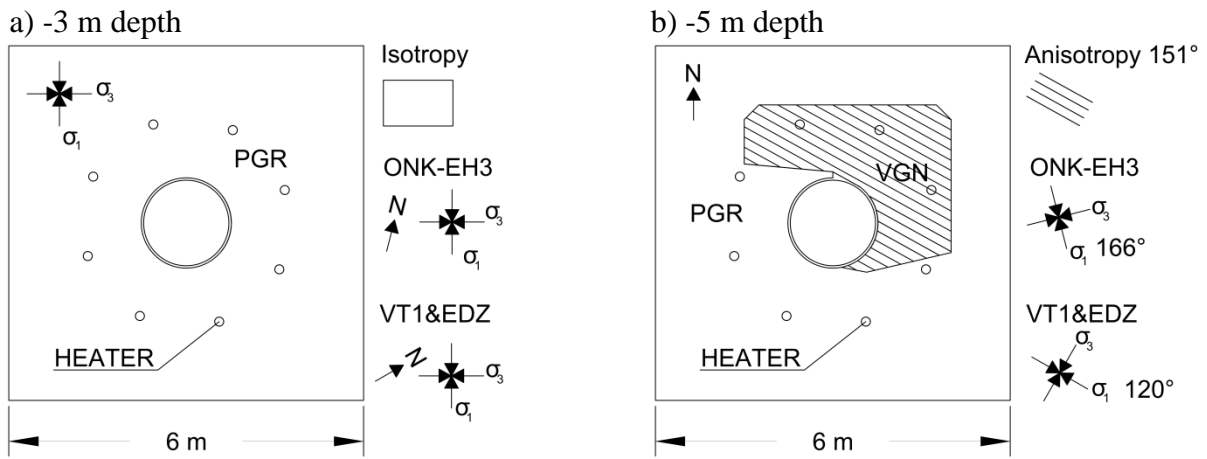


Fig. 5. Conceptual visualizations of models used. The model at -3 m depth is run with and without concrete in order to investigate the support effects.

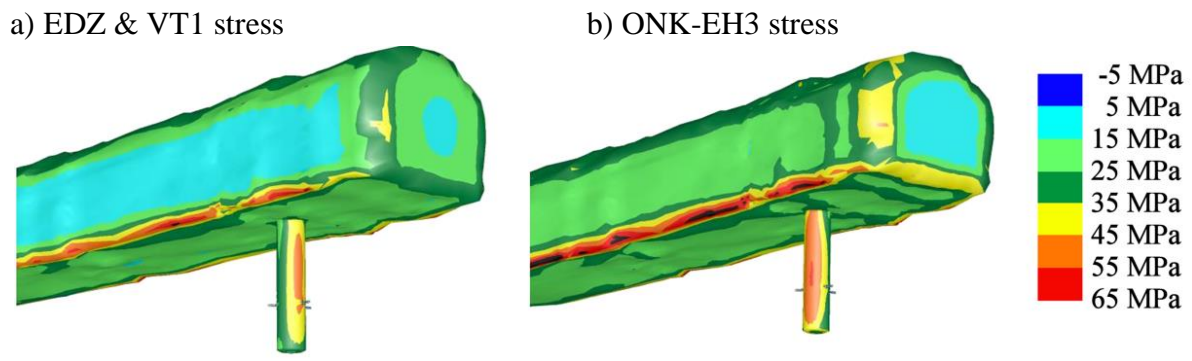


Fig. 6. Maximum principal stress distributions for two different stress interpretations EDZ & VT1 and ONK-EH3 (modified after Hakala & Valli (2013)).

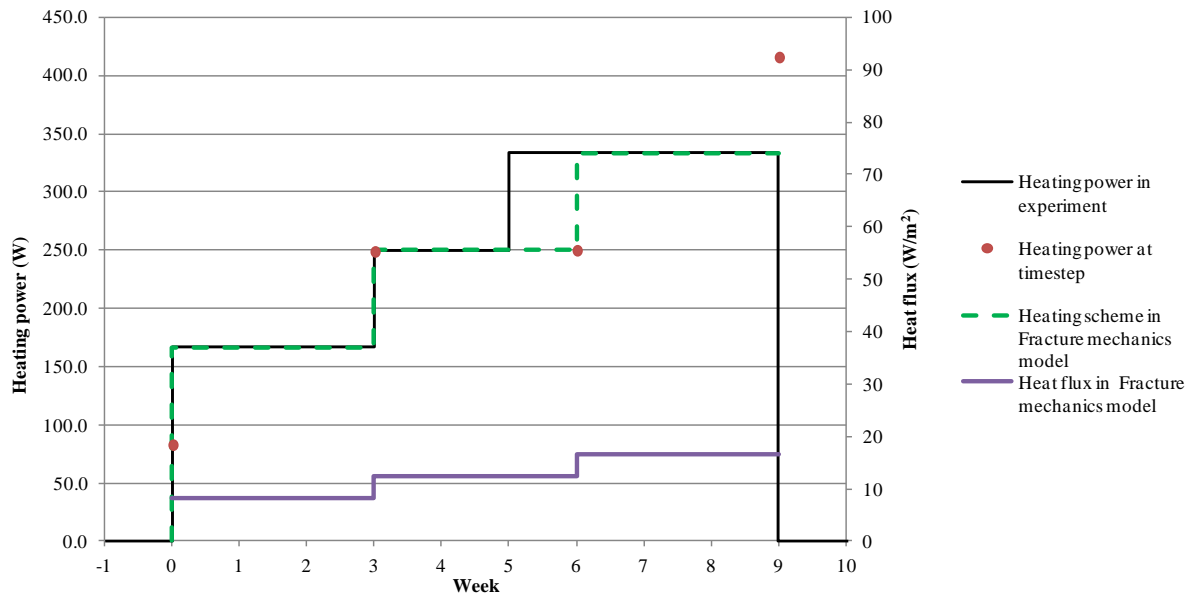


Fig. 7. Heating scheme in the experiment and the one used in fracture mechanics prediction with individual heating powers at timesteps and heat flux in the fracture mechanics prediction.

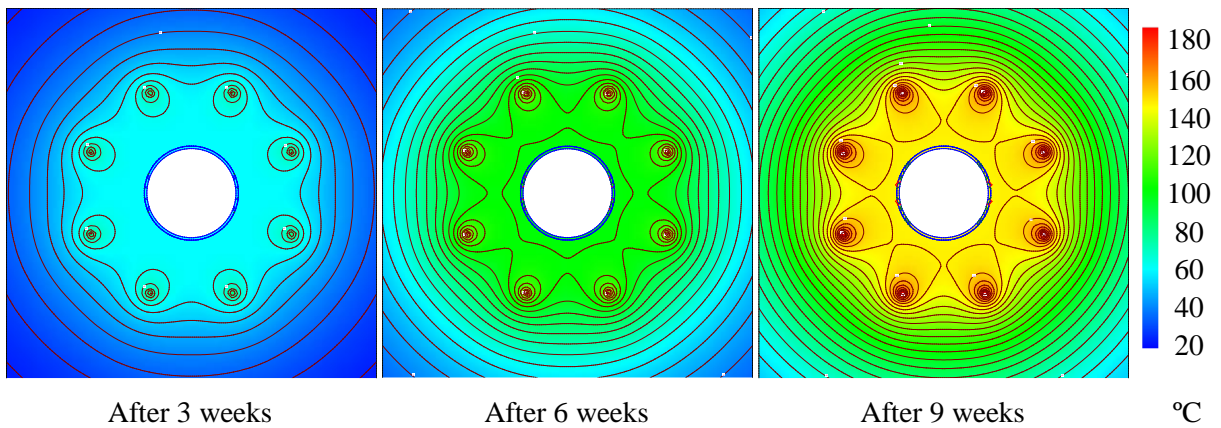


Fig. 8. Temperature distribution during the experiment modelled with Fracod 2D.

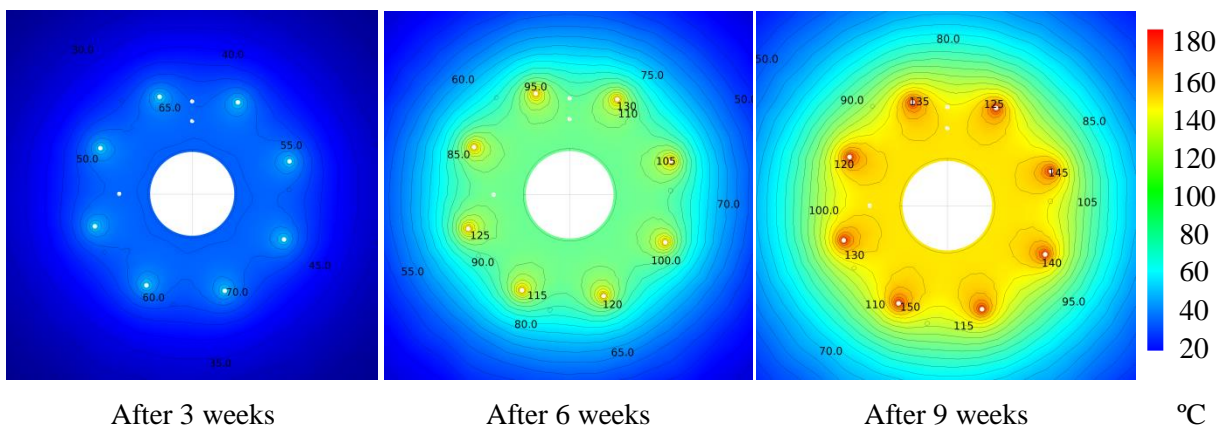


Fig. 9. Temperature distribution during the experiment modelled with Comsol 3D.

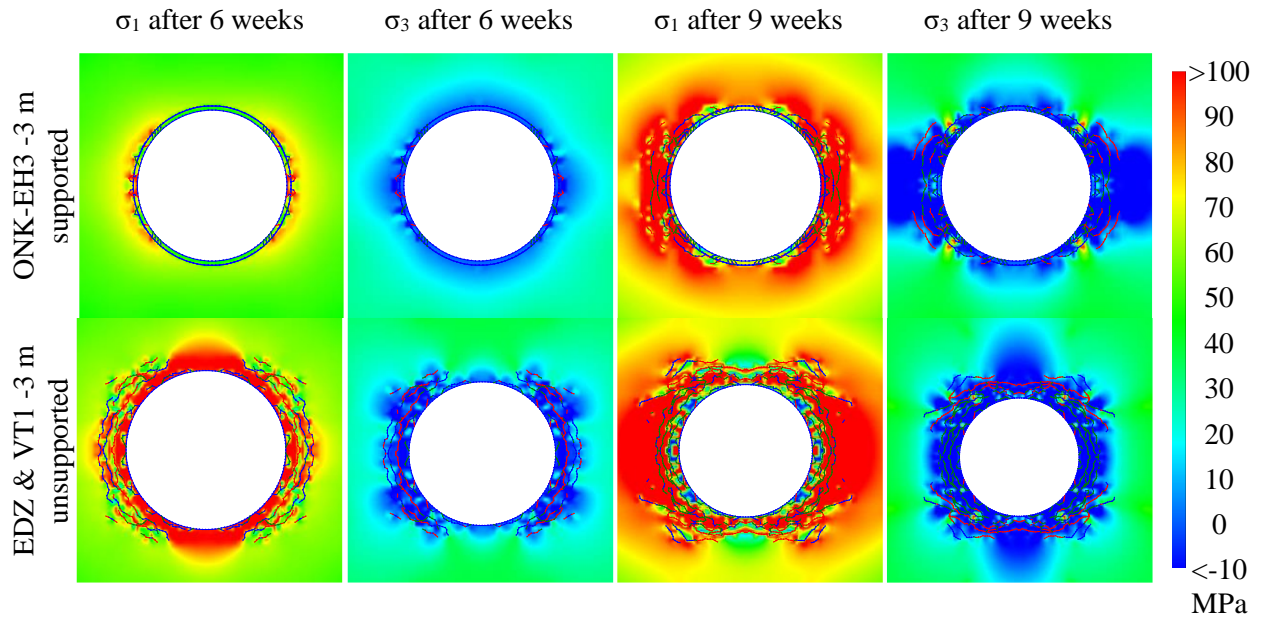


Fig. 10. Major and minor principal stresses in the calculation cases.

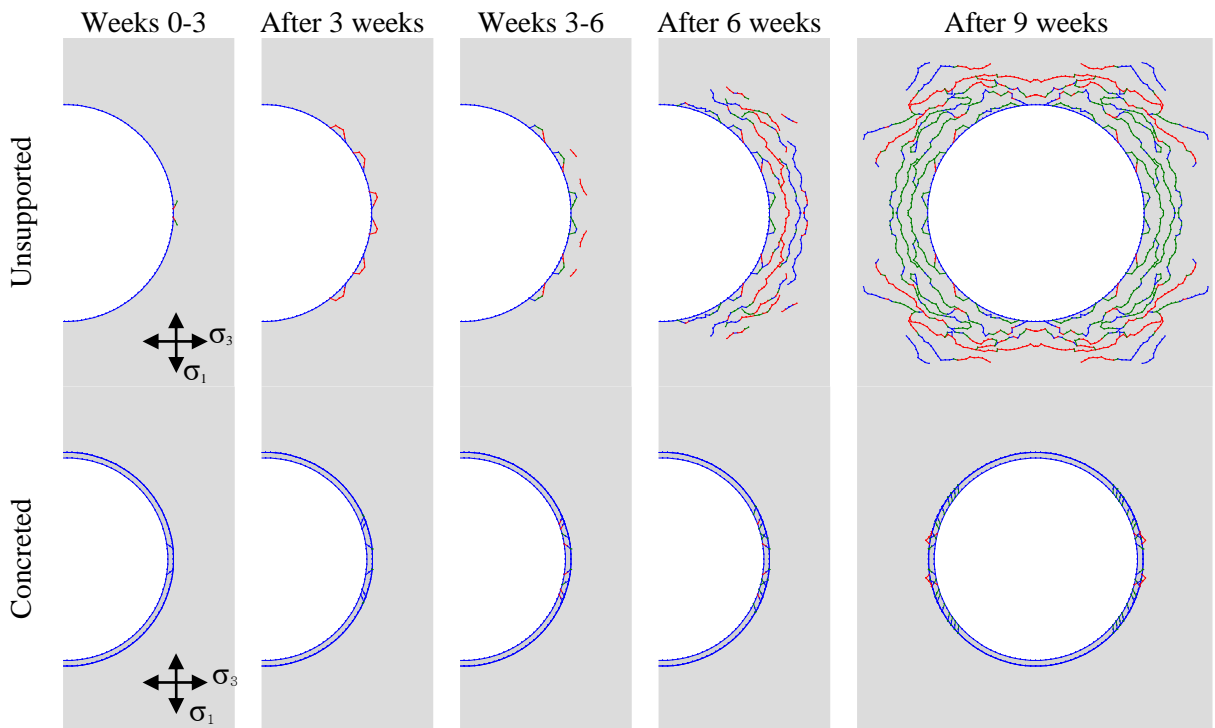


Fig. 11. Fracture propagation for the EDZ & VT1 stress state at -3 m depth.

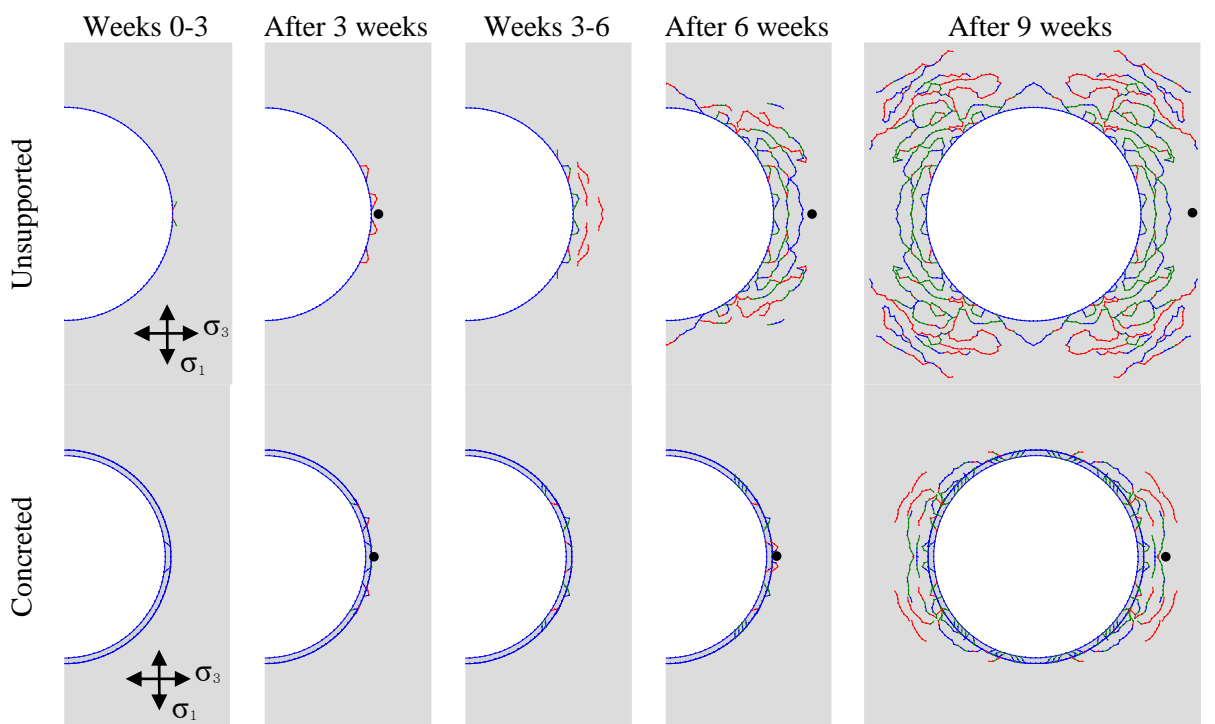


Fig 12. Fracture propagation for the ONK-EH3 stress state at -3 m depth. The points with maximum tangential stresses in intact rock are marked with black dots.

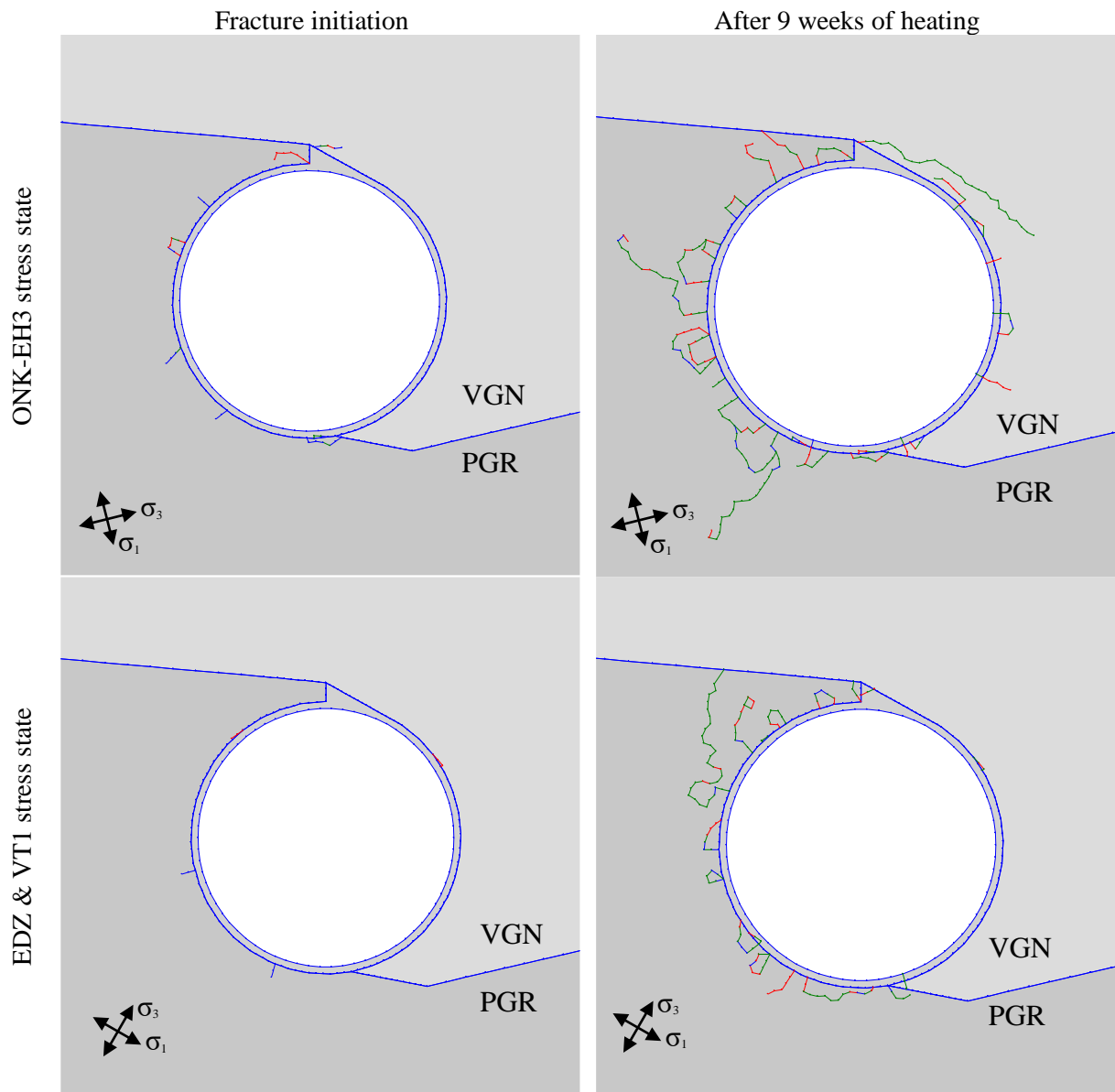


Fig. 13. Fracturing at -5 m depth for different calculation times and cases.

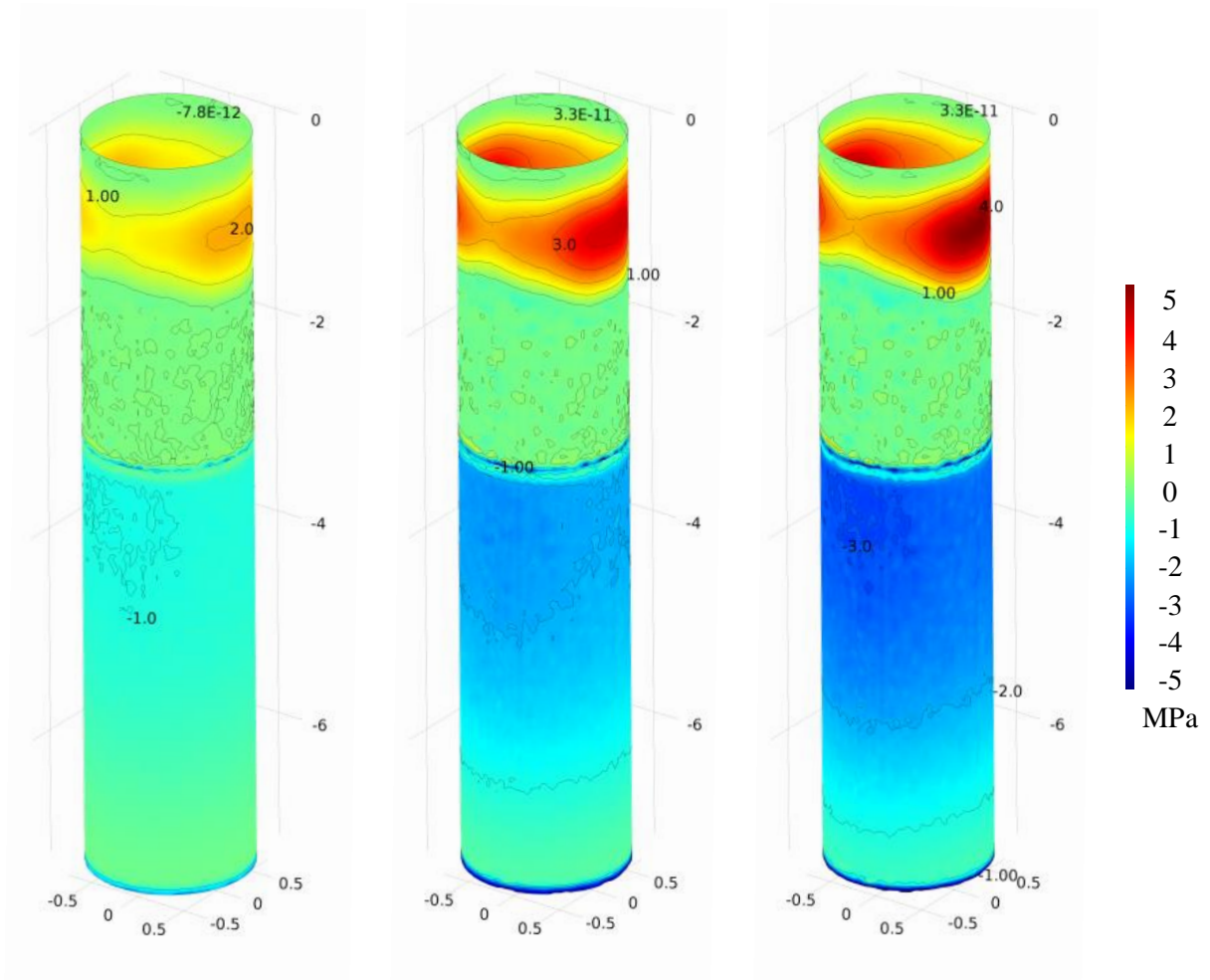


Fig 14. Support pressure after 3, 6 and 9 weeks for the ONK-EH3 case.

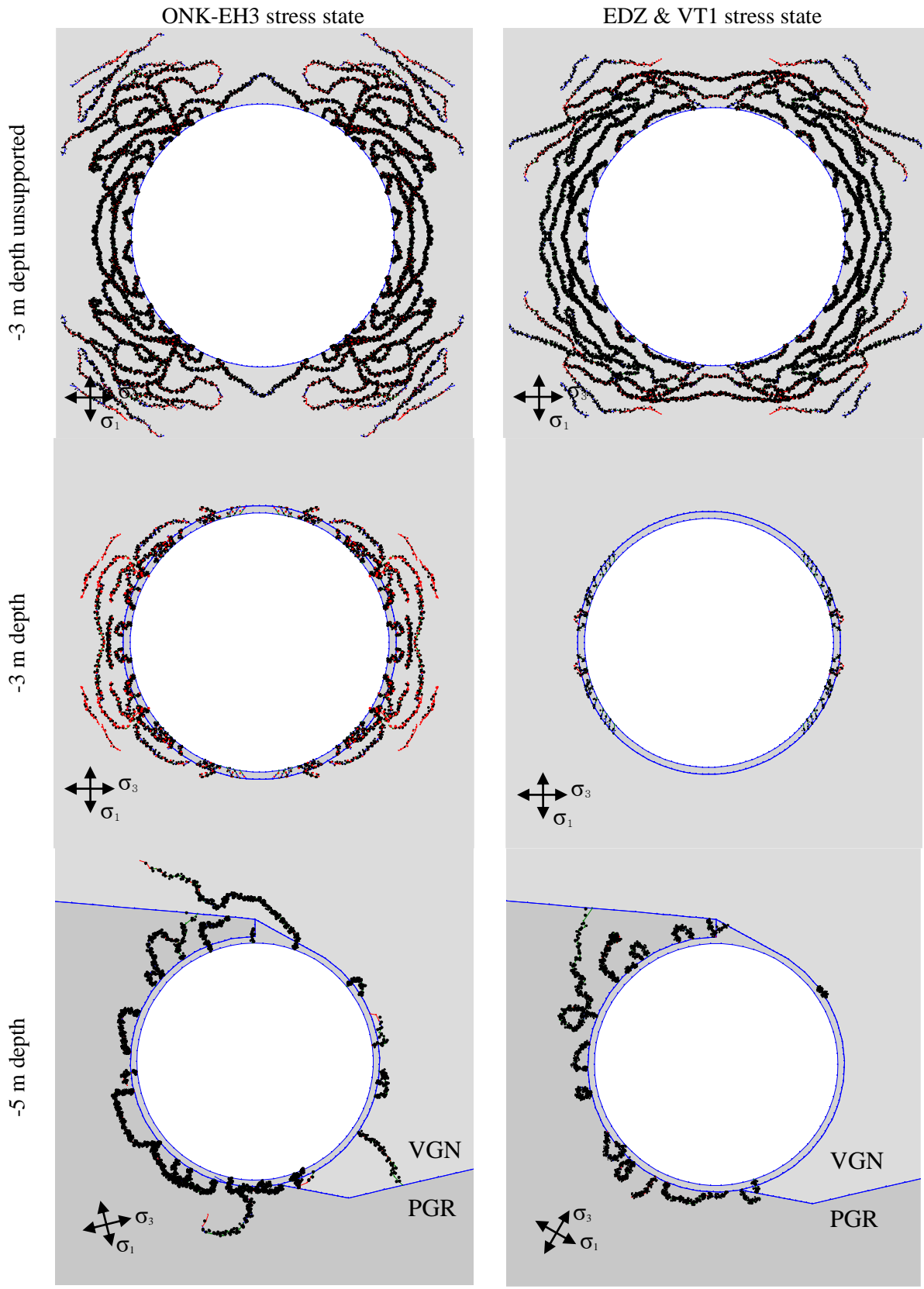


Fig 15. Predicted acoustic emission patterns for different calculation cases.

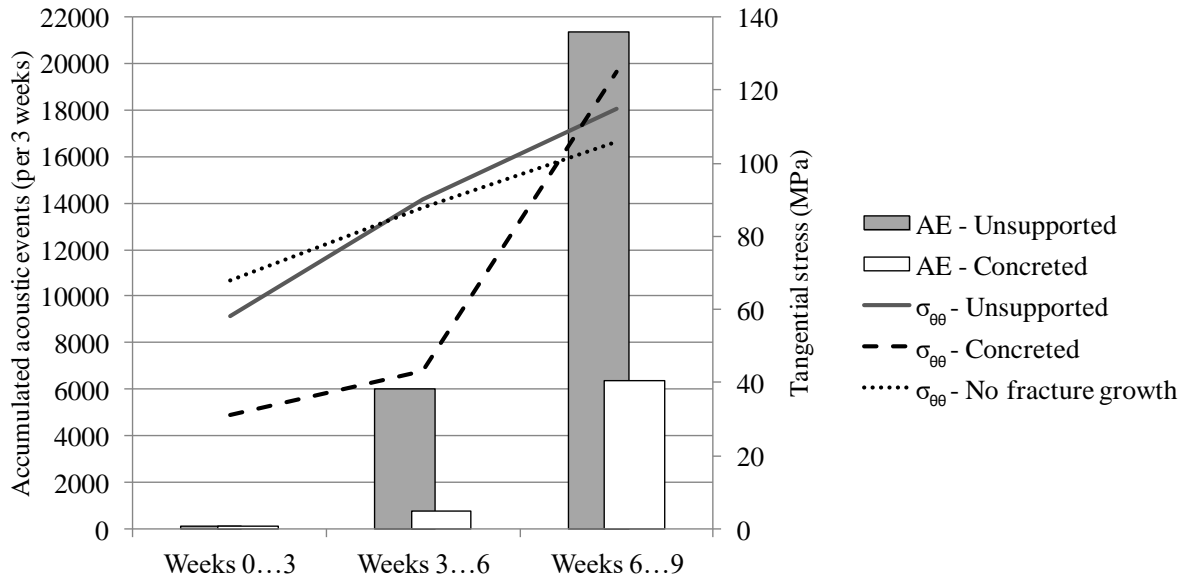


Fig 16. Predicted cumulative distribution of acoustic emission patterns and effective tangential stresses behind intact the rock surface for the ONK-EH3 case at -3 m depth.

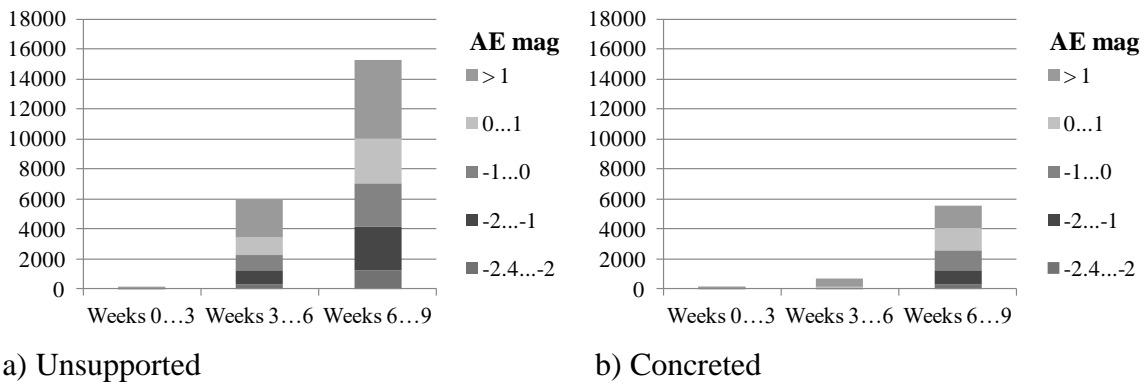


Fig 17. Predicted acoustic emission magnitudes for the ONK-EH3 case at -3 m depth with unsupported on the left and the supported case on the right.

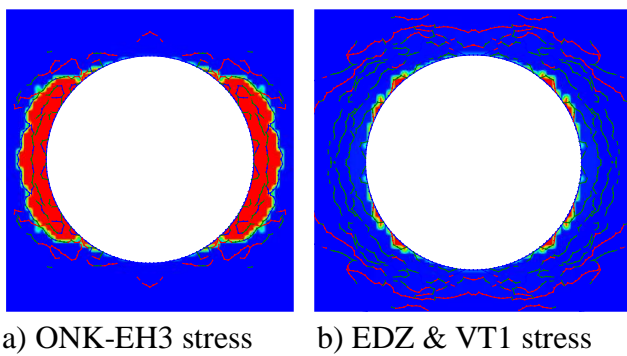


Fig. 18. Predicted loose blocks marked with red for unsupported cases at -3 m depth.

Table 1. Secondary rock stresses for different interpretations below the tunnel at experiment hole location. Calculated after Hakala & Valli (2013).

Stress interpretation	σ_1	σ_2	σ_3	σ_1 dir.
EDZ & VT1 -3 m	25.1 MPa	21.5 MPa	4.0 MPa	166°
EDZ & VT1 -5 m	27.4 MPa	20.6 MPa	6.0 MPa	166°
ONK-EH3 -3 m	23.0 MPa	15.0 MPa	3.0 MPa	120°
ONK-EH3 -5 m	22.0 MPa	15.0 MPa	5.0 MPa	120°

Table 2. Plane stresses used in modelling.

Stress interpretation	σ_{xx}	σ_{yy}	τ_{xy}
EDZ & VT1 -5 m	25.7 MPa	22.3 MPa	2.94 MPa
ONK-EH3 -5 m	15.41 MPa	21.59 MPa	1.64 MPa

Table 3. Material properties.

Property	PGR	PGR	VGN	concrete C35-3/45-1
Elastic modulus	53 GPa ^(a) , RM	53 GPa ^(a) , RM	53 GPa ^(a) , RM	34 GPa ^(d)
Poisson's ratio	0.25 ^(b) , RM	0.29 ^(b) , PGR, *	0.25 ^(b) , VGN	0.20 ^(d)
Density	2635 kg/m ³ ^(c) , PGR	2635 kg/m ³ ^(c) , PGR	2741 kg/m ³ ^(c) , VGN	2200 kg/m ³ ^(e)
Thermal capacity	689 J/kgK ^(c) , PGR	689 J/kgK ^(c) , PGR	725 J/kgK ^(c) , VGN	840 J/kgK ^(g)
Thermal conductivity	3.20 W/mK ^(c) , PGR	3.20 W/mK ^(c) , PGR	2.83 W/mK ^(c) , VGN	1.70 W/mK ^(f)
Lin. thermal expansion	7.2e-6 K ⁻¹ ^(b) , PGR	7.2e-6 K ⁻¹ ^(b) , PGR	9.7e-6 K ⁻¹ ^(b) , VGN	10e-6 K ⁻¹ ^(d)

^(a) Hakala & Valli 2012 ^(b) Posiva 2012 ^(c) Kukkonen *et al.* 2011 ^(d) EN 1992-1-1:2004 ^(e) based on quality assurance tests ^(f) Neville 1995 ^(g) SRMK C4: 2003 ^{RM} Rock mass property (estimated or mean) ^{PGR} Pegmatitic granite property ^{VGN} Veined gneiss property * Insufficient number of data (n=13)

Table 4. Fracture mechanics modelling parameters.

Property	PGR	VGN parallel	VGN perpend.	concrete C35-3/45-1
Cohesion	12.9 MPa ^(a)	12.4 MPa ^(a)	13.8 MPa ^(a)	17.5 MPa ^(c)
Friction angle	47° ^(a)	45° ^(a)	47° ^(a)	1° ^(c)
Tensile strength	12 MPa ^(a)	10 MPa ^(a)	14 MPa ^(a)	2.2 MPa ^(c)
Mode I fracture toughness	1.96 MPam ^{-0.5} ^(a)	1.87 MPam ^{-0.5} ^(a)	3.05 MPam ^{-0.5} ^(a)	0.31 MPam ^{-0.5} ^(d)
Mode II fracture toughness	3.30 MPam ^{-0.5} ^(a)	3.00 MPam ^{-0.5} ^(a)	3.86 MPam ^{-0.5} ^(a)	1.84 MPam ^{-0.5} ^(e)
Cohesion for fractures	10 MPa ^(a)	10 MPa ^(a)	10 MPa ^(a)	10 MPa ^(a)
Friction angle for fractures	35° ^(b)	35° ^(b)	35° ^(b)	35° ^(b)
Dilatation angle for fractures	2.5° ^(b)	2.5° ^(b)	2.5° ^(b)	2.5° ^(b)
Normal stiffness for fractures	20,000 GPa/m ^(a)	20,000 GPa/m ^(a)	20,000 GPa/m ^(a)	20,000 GPa/m ^(a)
Shear stiffness for fractures	2,000 GPa/m ^(a)	2,000 GPa/m ^(a)	2,000 GPa/m ^(a)	2,000 GPa/m ^(a)

^(a) Siren 2011 and 2012 ^(b) assumed after Posiva 2012 ^(c) EN 1992-1-1:2004 ^(d) using equation 1 derived after Davies (1988) and Reinhart *et al.* (1997) ^(e) calculated after relation by Reinhart *et al.* (1997)

Table 5. Maximum support pressure by concrete in intact parts.

Property	After 3 weeks	After 6 weeks	After 9 weeks
ONK-EH3 -3 m	1.3 MPa	1.9 MPa	-
EDZ & VT1 -3 m	1.9 MPa	2.4 MPa	3.0 MPa ¹
ONK-EH3 -5 m	1.5 MPa	- ²	- ²
EDZ & VT1 -5 m	-	- ²	- ²

¹ Only 90 degrees of intact concrete ² Models are not numerically stable